

# Dual-Scale Antenna Deployment for Pinching Antenna Systems

Xu Gan, *Member, IEEE*, Zhaolin Wang, *Member, IEEE*, Yuanwei Liu, *Fellow, IEEE*

**Abstract**—A dual-scale deployment (DSD) framework for pinching antenna systems (PASS) is proposed. 1) In the first coarse stage, the pinching antenna (PA) is transferred over a large-scale range at the waveguide level. 2) The refinement stage performs small-scale relocation of the PA with high precision. Four PA deployment protocols are provided in the proposed DSD framework. Then, a practical power consumption model is proposed, based on which the theoretical energy efficiency formulas for PASS are derived. The transmit precoding, PA radiation power, and PA deployment are jointly optimized to maximize the energy efficiency under the provided PA deployment protocols. To solve this non-convex, highly coupled problem, a low-complexity penalty-based alternating optimization algorithm is proposed. Simulation results validate the accuracy of theoretical results and the convergence of the proposed algorithm. It is demonstrated that: 1) PASS delivers about 70% higher energy efficiency than the conventional cell-free architecture and nearly *twofold* improvement relative to MIMO systems; 2) it is essential to specify the DSD resolution and deployment protocol to achieve the maximum energy efficiency for PASS.

**Index Terms**—Beamforming, dual-scale antenna deployment, energy efficiency, pinching antenna system, protocol design.

## I. INTRODUCTION

THE advent of sixth-generation (6G) wireless systems is anticipated to impose far more stringent requirements on spectral efficiency and full-dimensional coverage [1]. To meet these demands, emerging technologies such as reconfigurable intelligent surfaces [2], [3], fluid antennas [4], [5], and movable antennas [6] have shown promising performance improvements. These flexible antenna technologies advance transceiver architectures and enable environmental reconfigurability, which allows for controllable signal shaping. However, the potential benefits of these technologies are limited as they do not fully mitigate the performance degradation caused by large-scale fading.

Recently, pinching antenna systems (PASS) [7]–[9] have gained significant attention for their ability to boost spectral efficiency by enabling near-wire communications. Specifically in PASS, the dielectric waveguide serves both as the transport medium and the antenna rail, while small dielectric particles are pinched onto the waveguide to form pinching antennas (PAs), which act as programmable leakage points for signal radiation. Compared with prior flexible-antenna approaches, PASS directs part of the signal propagation through low-attenuation waveguides and radiates it closer to users, thereby reconfiguring large-scale fading and significantly reducing path loss. This additional spatial degree-of-freedom (DoF)

allows for the optimization of PA deployment and power radiation, enabling PA beamforming to shape the emitted field. These capabilities enhance the communication service quality, such as facilitating unobstructed communication links [10] and improving physical-layer security [11], [12]. Therefore, PA technology has drawn tremendous attention from both academia and industry [13], and is expected to play an important role in future wireless communications.

### A. Prior Works

Motivated by the aforementioned favorable characteristics of PASS, substantial research has been conducted to optimize the design of PA power radiation and deployment [14]–[19], aiming to fully exploit the additional DoFs introduced by PA and achieve performance gains in PASS. Studies on the PA power radiation typically categorize the methods into general, equal, and proportional power allocation, while PA deployment techniques are generally classified into discrete, continuous, and semi-continuous activation modes.

More specifically, the authors of [14] introduced both equal-power and proportional-power radiation schemes under a physics-based hardware model, formulating a transmit power minimization problem that jointly optimizes transmit and pinching beamforming. Due to its simplicity, the equal-power radiation approach was adopted in [15] and [16], where it was applied to multicast scenarios, with pinching beamforming designed to maximize the multicast rate. In contrast, the general-power scheme offers more flexibility in power allocation across PAs with the potential for higher performance, although its hardware implementation is more complex. For instance, a general-power radiation scheme was proposed in [17], yielding significant transmit power savings compared to the equal-power approach. In terms of PA deployment optimization, a practical strategy involves pre-deploying a large number of PAs and discretely activating a subset to serve communication users. In this regard, the authors of [18] formulated a transmit power minimization problem that optimizes transmit beamforming, pinching beamforming, and the number of active PAs, while ensuring the rate constraint of individual users is met. Additionally, the authors of [19] proposed three practical PA placement schemes, i.e., edge-deployment, center-deployment, and diagonal-deployment. Based on these PA deployment schemes, they investigated the performance of a novel simultaneous wireless information and power transfer system. Furthermore, continuous PA activation methods have been investigated in [14]–[17] to maximize system performance by optimizing PA deployment within the waveguide region, subject to the constraint that the distance between any two PAs exceeds a minimum threshold.

The authors are with the Department of Electrical and Electronic Engineering, The University of Hong Kong, Hong Kong (e-mail: {eee.ganxu, zhaolin.wang, yuanwei}@hku.hk).

## B. Motivations and Contributions

Although extensive studies have explored the substantial performance gains from continuous PA deployment, its practical adoption still faces two key concerns. First, under the existing hardware platforms, the practical implementation of continuous PA deployment cannot achieve the ideal combination of both wide-range and high-precision deployment. This limitation arises because the motor-driven device inherently involves a trade-off between travel range and spatial precision within a limited response time. Second, the power consumption associated with continuous PA deployment can be substantial, which may degrade the overall energy efficiency.

To effectively address these concerns, we propose a dual-scale deployment (DSD) framework that employs a hierarchical design for PA deployment. In the proposed framework, each PA is physically housed in a mobile base that slides on the waveguide, while the PA itself is tunable within the base. This architecture naturally decouples the PA deployment into two-stage operations, ensuring both wide-range repositioning and high-precision refinement. Based on the proposed DSD framework, we design an energy-efficient algorithm for joint optimization of the transmit precoding, PA power radiation, and PA deployment. The main contributions of this paper are summarized as follows:

- We propose the DSD framework for PA deployment in PASS. In the proposed DSD framework, the mobile base executes large-scale sliding in the coarse stage, while the PA performs small-scale tuning in the refinement stage. We provide four distinct implementation protocols within the DSD framework, namely: “base sliding then PA tuning (STT)”, “base selection then PA activation (STA)”, “base selection and PA tuning (SAT)”, and “base selection and PA activation (SAA)”, along with their respective advantages and limitations.
- We propose a realistic PASS power consumption model. Based on the proposed model, we derive closed-form theoretical expressions for energy efficiency in the DSD framework. Then, we formulate an energy efficiency maximization problem to jointly optimize the transmit precoding, PA radiation power, and PA deployment under four implementation protocols.
- We propose a novel low-complexity algorithm to efficiently address the energy efficiency maximization problem. In particular, we solve the PA deployment optimization by decoupling it into two independent subproblems in the DSD framework, i.e., optimizing the coarse-stage base placement and refinement-stage PA deployment. The proposed algorithm also incorporates Lagrangian transformations and block coordinate manifold optimization to tackle the transmit precoding and PA power radiation problems.
- We provide comprehensive numerical results to validate the accuracy of derived theoretical results and the convergence of the proposed algorithm. Numerical results also demonstrate that: 1) PASS delivers about 70% higher energy efficiency than the conventional cell-free architecture and nearly a twofold improvement relative to MIMO

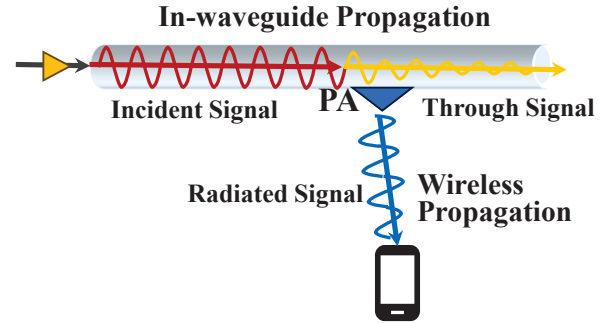


Fig. 1: The concept of PASS signal propagation.

systems; 2) the impact of DSD resolutions on energy efficiency is more pronounced in multi-PA systems; 3) the STT protocol provides over 80% improvement in energy efficiency due to the sliding-tuning gain, while the SAT protocol delivers the highest energy efficiency among the four protocols.

## C. Organization and Notations

The remainder of this paper is structured as follows. Section II provides the signal model for PASS and four implementation protocols in the DSD framework. Section III introduces the system model and formulates the energy efficiency maximization problem for PASS. Section IV details the proposed penalty-based alternating algorithm for joint optimization of the transmit precoding, PA power radiation, and PA deployment under the four implementation protocols. Numerical results evaluating the performance of different methods under various system configurations are presented in Section V. Finally, Section VI concludes the paper.

*Notations:* Scalars, vectors, and matrices are denoted by lower-case, bold-face lower-case, and bold-face upper-case letters, respectively. The sets of complex and real numbers are represented by  $\mathbb{C}$  and  $\mathbb{R}$ , respectively. The transpose, conjugate transpose, inverse, and trace operations are represented by  $(\cdot)^T$ ,  $(\cdot)^H$ ,  $(\cdot)^{-1}$ , and  $\text{tr}(\cdot)$ , respectively. The absolute value and Euclidean norm are indicated by  $|\cdot|$  and  $\|\cdot\|$ , respectively. The symbol  $\circ$  denotes element-wise multiplication. The expectation operator is denoted by  $\mathbb{E}[\cdot]$ . The real part of a complex number is denoted by  $\Re\{\cdot\}$ .  $\mathbf{I}_N$  denotes an identity matrix of size  $N \times N$ , and  $\mathbf{1}_N = [1, 1, \dots, 1]^T \in \mathbb{R}^{N \times 1}$ .  $[\mathbf{A}]_{m,n}$  represent the  $m$ -th row and  $n$ -th column element of  $\mathbf{A}$ . The  $\text{blkdiag}\{\mathbf{x}_1, \mathbf{x}_2, \dots, \mathbf{x}_M\}$  denotes a block diagonal matrix with diagonal blocks  $\mathbf{x}_1, \mathbf{x}_2, \dots, \mathbf{x}_M$ .

## II. DUAL-SCALE DEPLOYMENT PROTOCOLS FOR PASS

In this section, we first present the basic signal model for PASS, based on which four distinct implementation protocols in the DSD framework for PA deployment are introduced.

### A. Signal Model for PASS

Fig. 1 illustrates a simple PASS featuring a waveguide and a PA, where the incident signal into the waveguide is divided into the radiated and through signals at the PA. To characterize this PA feature, let  $s_{n-1}^t$  denote the signal

transmitted towards the  $n$ -th PA, where  $n \in \{1, 2, \dots, N\}$ ,  $s_0^t$  denotes the original signal fed into the waveguide, and  $N$  denotes the total number of PAs. In particular, the signal  $s_{n-1}^t$  will travel through the waveguide of distance  $L_n^i$  and reach the  $n$ -th PA, which is modeled as the incident signal  $s_n^i$ . Due to the finite conductor resistance and dielectric loss of the waveguide, the mathematical relationship between  $s_{n-1}^t$  and  $s_n^i$  can be modeled as the following energy attenuation expression [Eq. (8-47), 20] as

$$s_n^i = \exp(-\gamma_g L_n^i) \cdot s_{n-1}^t. \quad (1)$$

Here  $\gamma_g$  is the in-waveguide attenuation constant defined as  $\gamma_g = \alpha_g + j\beta_g$ , where  $\alpha_g$  and  $\beta_g$  denote the positive-value amplitude and phase constants, respectively. The values of  $\alpha_g$  and  $\beta_g$  are determined by waveguide parameters and the signal wavelength, which can be obtained via the Eqs. (8-48) and (8-49) of the work [20], respectively. In particular,  $\beta_g$  can be approximated by  $\omega_g \sqrt{\mu_g \epsilon_g}$  [20], consistent with the in-waveguide signal model [8] as  $\beta_g = \frac{2\pi}{\lambda_g}$ , where  $\lambda_g = \frac{2\pi}{\omega_g \sqrt{\mu_g \epsilon_g}}$  is the effective signal wavelength in the waveguide medium. As such, the incident signal at the  $n$ -th PA is expressed as

$$s_n^i = \exp\left(-\left(\alpha_g + j\frac{2\pi}{\lambda_g}\right)L_n^i\right) s_{n-1}^t. \quad (2)$$

The  $n$ -th PA attached to the waveguide radiates part of the energy through electromagnetic coupling, while the remaining signal continues to transmit through the waveguide. Let  $s_n^r$  and  $s_n^t$  represent the radiated and through signals at the  $n$ -th PA, respectively, and can be modeled [14] as

$$s_n^r = \sqrt{\delta_n} s_n^i, \quad (3)$$

where  $\delta_n \in [0, 1]$ . According to the law of energy conservation, the sum of the power of radiated and through signals has to be equal to the incident signal power, i.e.,  $|s_n^r|^2 + |s_n^t|^2 = |s_n^i|^2$ , which yields

$$s_n^t = \sqrt{1 - \delta_n} s_n^i. \quad (4)$$

Then, the through signal propagates towards the  $(n+1)$ -th PA along the waveguide and serves as the next incident signal  $s_{n+1}^i$ . On the other hand,  $s_n^r$  is transmitted via wireless propagation to serve communication users. Let  $h_{nk}$  denote the wireless channel between the  $n$ -th PA and the  $k$ -th single-antenna user (or  $\mathbf{h}_{nk}$  for the multi-antenna user). The received signal at the  $k$ -th user from the  $n$ -th PA radiation is given by

$$y_{nk} = h_{nk} s_n^r + n_k, \quad (5)$$

where  $n_k$  is the additive white Gaussian noise  $\mathcal{CN}(0, N_0)$  and  $N_0$  is the noise power. As a simple example, the wireless channels in PASS can be modeled by a free-space line-of-sight (LoS) channel as [8], [14]

$$h_{nk} = \sqrt{\frac{c^2}{16\pi^2 f_c^2} \frac{e^{-j\frac{2\pi}{\lambda} r_{nk}}}{r_{nk}}}, \quad (6)$$

where  $c$  is the light speed,  $f_c$  and  $\lambda$  are the carrier frequency and wavelength, respectively, and  $r_{nk}$  is the distance between the  $n$ -th PA and  $k$ -th user. Substituting Eqs. (2)-(4), and (6) into (5), the received signal at the  $k$ -th user from  $N$  PAs is

further expressed as

$$y_k = \sum_{n=1}^N \sqrt{\frac{c^2}{16\pi^2 f_c^2} \frac{\sqrt{\xi_n}}{r_{nk}}} \times \exp\left(-\alpha_g d_n - j\left(\frac{2\pi}{\lambda} r_{nk} + \frac{2\pi}{\lambda_g} d_n\right)\right) s_0^t + n_k. \quad (7)$$

where  $\xi_n = \delta_n \prod_{j=1}^{n-1} (1 - \delta_j)$  and  $d_n = \sum_{j=1}^n L_j^i$  denote the overall radiation power coefficient and in-wavelength propagation length for the  $n$ -th PA. Let  $P_k^d$  denote the received desired-signal power of the  $k$ -th user, where

$$P_k^d = \left| \sum_{n=1}^N \sqrt{\frac{c^2}{16\pi^2 f_c^2} \frac{\sqrt{\xi_n}}{r_{nk}}} \exp\left(-\alpha_g d_n - j\left(\frac{2\pi}{\lambda} r_{nk} + \frac{2\pi}{\lambda_g} d_n\right)\right) \right|^2. \quad (8)$$

This expression shows that  $P_k^d$  is jointly determined by the PA power radiation coefficients  $\{\zeta_n\}_{n=1}^N$  and the PA deployment through  $\{r_{nk}, d_n\}_{n=1}^N$ . Thus, maximizing the received desired-signal power requires joint optimization of PA power radiation and PA deployment. Strategies for allocating PA radiation power, including the equal- and proportional-power models, have been introduced and analyzed in [14]. In contrast, practical protocols for adjusting PA position remain underexplored. To bridge this gap, in the following part, we develop four implementation protocols in the DSD framework for PA deployment in PASS.

#### B. Four Implementation Protocols in the DSD Framework

As shown in (8), the deployment of the  $n$ -th PA simultaneously affects the amplitude and phase of  $P_k^d$ , through  $d_n$  and  $r_{nk}$ . Thus, it is very difficult to obtain the optimal PA deployment that maximizes  $P_k^d$ , as the underlying optimization is highly non-convex and exhibits strong coupling among the  $N$  PAs. To solve these challenges, we divide the effect of PA deployment on  $P_k^d$  into amplitude and phase components, respectively, as

$$a_{nk}(\mathbf{p}_n) = (r_{nk}(\mathbf{p}_n))^{-1} \exp(-\alpha_g d_n(\mathbf{p}_n)), \quad (9)$$

$$\theta_{nk}(\mathbf{p}_n) = \frac{2\pi}{\lambda} r_{nk}(\mathbf{p}_n) + \frac{2\pi}{\lambda_g} d_n(\mathbf{p}_n), \quad (10)$$

where  $\mathbf{p}_n$  denotes the position of the  $n$ -th PA. Then, the desired-signal power problem with respect to (w.r.t.) PA deployment can be rewritten as

$$\max_{\mathbf{p}_n \in \mathcal{G}_n} \left| \sum_{n=1}^N \sqrt{\frac{c^2 \xi_n}{16\pi^2 f_c^2}} a_{nk}(\mathbf{p}_n) \exp(-j\theta_{nk}(\mathbf{p}_n)) \right|^2, \quad (11)$$

where  $\mathcal{G}_n$  denotes the deployment range of the  $n$ -th PA along the waveguide.

It can be observed that the challenge of solving problem (11) lies in the coupling between  $a_{nk}$  and  $\theta_{nk}$ ,  $\forall n$ . To solve this, we propose a two-stage optimization method. The insight behind this method is that a small variation of the PA position  $\Delta \mathbf{p}_n$  induces a negligible change in amplitude term  $a_{nk}(\mathbf{p}_n + \Delta \mathbf{p}_n)$ , but enables  $\theta_{nk}(\mathbf{p}_n + \Delta \mathbf{p}_n)$  to sweep the full range of  $[-\pi, \pi)$ . Hence,  $\theta_{nk}$  can be tuned by small PA movements with negligible amplitude perturbation, which validates the decoupling approximation and motivates the DSD framework.

In this way, we first solve the decoupled problem as

$$\max_{a_{nk}, \theta_{nk}} \left| \sum_{n=1}^N \sqrt{\frac{c^2 \xi_n}{16\pi^2 f_c^2}} a_{nk} \exp(-j\theta_{nk}) \right|^2, \quad (12)$$

where the range of variable  $a_{nk}$  is determined by the position of  $k$ -th user and  $\mathcal{G}_n$ .

Based on the optimal  $a_{nk}^{\text{opt}}$  and  $\theta_{nk}^{\text{opt}}$  derived from the problem (12), the proposed DSD strategy carries out coarse- and refinement-stage of the  $n$ -th PA deployment in a two-stage manner. Particularly, in the coarse stage, the  $n$ -th PA positioning is adjusted to  $\mathbf{p}_n^C$  to achieve the desired amplitude by solving

$$\mathbf{p}_n^C = \arg \min_{\mathbf{p}_n \in \mathcal{G}_n} \left| a_{nk}^{\text{opt}} - (r_{nk}(\mathbf{p}_n))^{-1} \exp(-\alpha_g d_n(\mathbf{p}_n)) \right|^2. \quad (13)$$

Then, in the refinement stage, the  $n$ -th PA will be further refined with  $\Delta \mathbf{p}_n^F$  to achieve the desired phase by solving

$$\Delta \mathbf{p}_n^F = \arg \min_{\Delta \mathbf{p}_n \in \Delta \mathcal{G}_n} \left| \theta_{nk}^{\text{opt}} - \left( \frac{2\pi}{\lambda} r_{nk}(\mathbf{p}_n^C + \Delta \mathbf{p}_n) + \frac{2\pi}{\lambda_g} d_n(\mathbf{p}_n^C + \Delta \mathbf{p}_n) \right) \right|^2, \quad (14)$$

where  $\Delta \mathcal{G}_n$  denotes the deployment range of the  $n$ -th PA within the base. After the proposed DSD operations, the final optimized position of the  $n$ -th PA is  $\mathbf{p}_n^F = \mathbf{p}_n^C + \Delta \mathbf{p}_n^F$ .

**Remark 1.** In the proposed DSD framework, the  $n$ -th PA is first transferred along the waveguide to a wide-range waypoint  $\mathbf{p}_n^C$  to mitigate large-scale path-loss, typically over several to tens of meters. It then performs a high-precision refinement to the final location  $\mathbf{p}_n^F$  to ensure small-scale fading-phase alignment, typically within several micrometers to a few millimeters. The proposed DSD framework reformulates PA deployment into two decoupled subproblems, which substantially reduces the computational complexity of the PASS designs. It can also be smoothly applied to a motorized actuator system to ensure both wide-range repositioning and high-precision refinement.

In practice, the proposed DSD framework can be realized by exploiting a hardware system integrating motorized and piezoelectric motors [21] from the Physik Instrument company. We can utilize its motorized module to enable wide-range movement to the coarse position, and its piezoelectric-based actuator to enable precise fine-tuning to the accurate position. As such, the  $n$ -th PA requires an operation time  $t_n = \frac{\|\mathbf{p}_n^C\|}{v_n^{MO}} + \frac{\|\Delta \mathbf{p}_n^F\|}{v_n^{PI}}$  during the actual position adjustment process, where  $v_n^{MO}$  and  $v_n^{PI}$  denote the motorized-based and piezoelectric-based movement speeds, respectively. Considering the common velocity metrics  $v_n^{MO} = 10$  m/s and  $v_n^{PI} = 10^{-2}$  m/s, it far exceeds the 10 ms NR frame structure [22]. Hence, practical PA deployment has a latency on the order of seconds, and therefore cannot support real-time adaptation to communication channels.

Fortunately, one simple and effective solution is to pre-deploy a large number of PAs and then activate a subset to achieve the same effect as adjusting the positions of PAs.

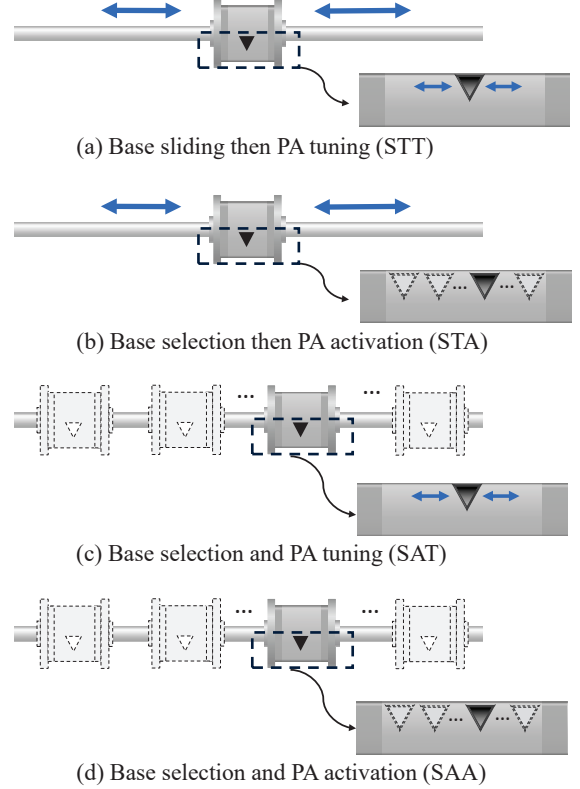


Fig. 2: Schematic diagram of four protocols in the proposed DSD framework.

Nevertheless, this also raises concerns about the performance degradation and hardware cost associated with pre-deploying a large number of PAs. For example, implementing centimeter-level positioning accuracy over 100 m would require  $10^4$  pre-deployed PAs. To strike a satisfactory trade-off between the number of pre-deployed PAs, positioning accuracy, and response time, we innovatively introduce four implementation protocols of the DSD framework as in Fig. 2.

- **STT:** Base sliding is carried out by a motorized module over a waveguide-level range for coarse-stage deployment. Fine-tuning PA inside the base is then performed by a piezoelectric module.
- **STA:** Base sliding is carried out by a motorized module over a waveguide-level range for coarse-stage deployment.  $N_A$  PAs are pre-deployed inside the base, where one PA is activated each time slot.
- **SAT:**  $N_B$  bases are pre-deployed along the waveguide, each equipped with a tunable PA. In each time slot, one base is selected, and the PA within that base is finely tuned by a piezoelectric module.
- **SAA:**  $N_B$  bases are pre-deployed along the waveguide, each containing  $N_A$  PAs. In each time slot, one base is selected, and one PA within that PB is activated.

In Table I, we summarize the response time, pre-deployed PA number, power consumption, and spectral efficiency of these four implementation protocols (a)-(d). Across the four implementation protocols, the PA deployment algorithm designs only differ in the search grid sets in Eqs. (13) and

Protocol	Response Time	Pre-deployed PA Number	Power Consumption	Spectral Efficiency
STT	Long	Small	Very High	High
STA	Moderate	Moderate	High	Moderate
SAT	Moderate	Moderate	Low	Moderate
SAA	Nearly zero	Large	Very Low	Low

TABLE I: Summary of performance metrics for four PA operating protocols.

(14). We next detail the protocol-specific grid constructions. For simplified mathematical modeling, we assume that the waveguide is deployed along the  $x$ -axis. This means that the PA deployment designs only require consideration of its  $x$ -coordinate. Let  $x^{\min}$  and  $x^{\max}$  denote the minimum and maximum coordinates of the base deployment range along the waveguide, respectively. We use  $\delta^C$  and  $\delta^F$  to indicate the position adjustment step sizes, or resolutions, of the sliding base and tuning PA, respectively. Besides, let  $L^F$  denote the length of PA's deployment range within each base in the refinement stage. As for the selection or activation representations, it is assumed that  $N \cdot N^F$  bases and  $N \cdot N^C$  PAs are pre-deployed, from which  $N$  bases or PAs are selected/activated in each time slot. Four practical implementations of the proposed DSD search grid set are provided as follows:

• **STT:**

$$\mathbf{x}^{CG} = \left\{ x^C \left| \begin{array}{l} x^C = x^{\min} + g^C \delta^C, \\ g^C = 0, 1, \dots, \frac{x^{\max} - x^{\min}}{\delta^C} \end{array} \right. \right\}, \quad (15)$$

$$\mathbf{x}^{FG} = \left\{ x^F \left| \begin{array}{l} x^F = -\frac{L^F}{2} + g^F \delta^F, \\ g^F = 0, 1, \dots, \frac{L^F}{\delta^F} \end{array} \right. \right\}. \quad (16)$$

• **STA:**

$$\mathbf{x}^{CG} = \left\{ x^C \left| \begin{array}{l} x^C = x^{\min} + g^C \delta^C, \\ g^C = 0, 1, \dots, \frac{x^{\max} - x^{\min}}{\delta^C} \end{array} \right. \right\}, \quad (17)$$

$$\mathbf{x}^{FG} = \left\{ x^F \left| \begin{array}{l} x^F = -\frac{L^F}{2} + g^F \frac{L^F}{NN^F}, \\ g^F = 0, 1, \dots, NN^F - 1 \end{array} \right. \right\}. \quad (18)$$

• **SAT:**

$$\mathbf{x}^{CG} = \left\{ x^C \left| \begin{array}{l} x^C = x^{\min} + g^C \frac{x^{\max} - x^{\min}}{NN^C}, \\ g^C = 0, 1, \dots, NN^C - 1 \end{array} \right. \right\}, \quad (19)$$

$$\mathbf{x}^{FG} = \left\{ x^F \left| \begin{array}{l} x^F = -\frac{L^F}{2} + g^F \delta^F, \\ g^F = 0, 1, \dots, \frac{L^F}{\delta^F} \end{array} \right. \right\}. \quad (20)$$

• **SAA:**

$$\mathbf{x}^{CG} = \left\{ x^C \left| \begin{array}{l} x^C = x^{\min} + g^C \frac{x^{\max} - x^{\min}}{NN^C}, \\ g^C = 0, 1, \dots, NN^C - 1 \end{array} \right. \right\}, \quad (21)$$

$$\mathbf{x}^{FG} = \left\{ x^F \left| \begin{array}{l} x^F = -\frac{L^F}{2} + g^F \frac{L^F}{NN^F}, \\ g^F = 0, 1, \dots, NN^F - 1 \end{array} \right. \right\}. \quad (22)$$

Here, the analytical expressions of  $\mathbf{x}^{CG}$  and  $\mathbf{x}^{FG}$  correspond to the  $x$ -axis of  $\mathcal{G}_n$  and  $\Delta\mathcal{G}_n$  in Eqs. (13) and (14), respectively, and can be easily extended to two or three dimensions. It is crucial to identify the optimal protocols (a)-(d) to achieve the best performance of PASS. In the subsequent sections, we will jointly optimize the transmit precoding, PA radiation power, and PA deployment under the four implementation protocols to maximize the energy efficiency of PASS.

### III. SYSTEM MODEL AND PROBLEM FORMULATION

Based on the basic signal model and the proposed DSD framework for PASS-enabled wireless communication, this section will investigate a general system model, where  $M$  waveguides are fed by  $M$  dedicated RF chains, each consisting of  $N$  PAs, cooperatively serving  $K$  users. Let  $\mathbf{q}_k = [x_k^U, y_k^U]^T$  and  $\mathbf{p}_{mn}$  denote the position coordinates of the  $k$ -th user and  $n$ -th PA on the  $m$ -th waveguide, respectively. The following subsection will provide a detailed analysis of the transmit signal with RF chain precoding, the received signal at the user side, and the system's energy efficiency.

#### A. Signal Model

Let  $s_k$  denote the information symbol for the  $k$ -th user with  $\mathbb{E}\{|s_k|^2\} = 1$ . After the  $m$ -th RF chain precodes  $s_k$  with weight  $w_{mk}$ ,  $\forall k$ , for the  $K$  users, the resulting signal fed into the  $m$ -th waveguide is give by

$$x_m = \sum_{k=1}^K w_{mk} s_k, \quad (23)$$

where the total transmit power of  $M$  RF chains is constrained by  $P_{\max}$ , i.e.,  $\mathbb{E}\left\{\sum_{m=1}^M |x_m|^2\right\} \leq P_{\max}$ .

The received signal of the  $k$ -th user comprises the radiated signal from the  $N$  PAs along each of the  $M$  waveguides, i.e.,

$$y_k = \sum_{m=1}^M \sum_{n=1}^N \sqrt{\xi_{mn}} g_{mn} h_{mnk} x_m + n_k, \quad (24)$$

where  $g_{mn}$  and  $h_{mnk}$  denote the in-waveguide channel of the  $n$ -th PA on the  $m$ -th waveguide, and wireless channel from the  $n$ -th PA on the  $m$ -th waveguide to the  $k$ -th user, respectively.  $\xi_{mn}$  is the radiation power coefficient of the  $n$ -th PA on the  $m$ -th waveguide, satisfying  $\sum_{n=1}^N \xi_{mn} = 1$ ,  $\forall m$ , and  $n_k \sim \mathcal{CN}(0, N_0)$  is the additive white Gaussian noise. More particularly, the in-waveguide channel is given by (c.f. (2))

$$g_{mn} = \exp\left(-\left(\alpha_g + j\frac{2\pi}{\lambda_g}\right) d_{mn}\right), \quad (25)$$

where  $d_{mn}$  is in-waveguide propagation distance for the  $n$ -th PA on the  $m$ -th waveguide. The wireless channel model combines both the LoS and NLoS links, i.e.,

$$h_{mnk} = \sqrt{C_0 r_{mnk}^{-\beta_u}} \left( \sqrt{\frac{K_r}{K_r + 1}} e^{-j\frac{2\pi}{\lambda} r_{mnk}} + \sqrt{\frac{1}{K_r + 1}} \tilde{h}_{mnk} \right), \quad (26)$$

where  $C_0$  and  $\beta_u$  denote the path-loss coefficient at the reference distance 1 m and the path-loss exponential coefficient, respectively,  $r_{mnk}$  is the distance from the  $n$ -th PA on the  $m$ -th waveguide to the  $k$ -th user,  $K_r \geq 0$  is the Rician factor to measure the power ratio between the LoS and NLoS links, and

$\tilde{h}_{mnk} \sim \mathcal{CN}(0, 1)$  represents NLoS links. It can be observed that the free-space LoS channel in (6) is a special case of our considered channel in (26), and becomes equivalent when  $K_r \rightarrow +\infty$ ,  $C_0 = \frac{c^2}{16\pi^2 f_c^2}$  and  $\beta_u = 2$ .

### B. Energy Efficiency

In practical communication systems, it is typically assumed that the BS has perfect channel state information (CSI), while users only possess statistical CSI. In this case, the effective SINR of the  $k$ -th user is given by [23]:

$$\gamma_k = \frac{|\text{DS}_k|^2}{\mathbb{E}\{|\text{CU}_k|^2\} + \sum_{i \neq k}^K \mathbb{E}\{|\text{UI}_{ki}|^2\} + N_0}, \quad (27)$$

where  $\text{DS}_k$ ,  $\text{CU}_k$ , and  $\text{UI}_{ki}$  denote the  $k$ -th user's desired signal, effective interference from the CSI uncertainty, and the other  $i$ -th user interference signals, respectively, given by

$$\text{DS}_k = \mathbb{E} \left\{ \sum_{m=1}^M \sum_{n=1}^N \sqrt{\xi_{mn}} g_{mn} h_{mnk} w_{mk} s_k \right\}, \quad (28)$$

$$\text{CU}_k = \sum_{m=1}^M \sum_{n=1}^N \sqrt{\xi_{mn}} g_{mn} h_{mnk} w_{mk} s_k - \text{DS}_k, \quad (29)$$

$$\text{UI}_{ki} = \sum_{m=1}^M \sum_{n=1}^N \sqrt{\xi_{mn}} g_{mn} h_{mnk} w_{mi} s_i. \quad (30)$$

The SINR expression (27) can be reformulated into a more compact matrix form as follows:

$$\gamma_k = \frac{|\bar{\mathbf{h}}_k^T \mathbf{\Xi} \mathbf{G} \mathbf{w}_k|^2}{\mathbb{E} \left\{ |\bar{\mathbf{h}}_k^T \mathbf{\Xi} \mathbf{G} \mathbf{w}_k|^2 \right\} + \sum_{i \neq k}^K \mathbb{E} \left\{ |\mathbf{h}_k^T \mathbf{\Xi} \mathbf{G} \mathbf{w}_i|^2 \right\} + N_0}, \quad (31)$$

where  $\bar{\mathbf{h}}_k \in \mathbb{C}^{MN \times 1}$ ,  $\mathbf{h}_k \in \mathbb{C}^{MN \times 1}$ , and  $\mathbf{h}_k \in \mathbb{C}^{MN \times 1}$  are the deterministic, stochastic and overall channels of wireless propagation from  $MN$  PAs to the  $k$ -th user, respectively, defined by

$$[\bar{\mathbf{h}}_k]_{(m-1)N+n} = \sqrt{C_0 r_{mnk}^{-\beta_u}} \sqrt{\frac{K_r}{K_r + 1}} e^{-j \frac{2\pi}{\lambda} r_{mnk}}, \quad (32)$$

$$[\mathbf{h}_k]_{(m-1)N+n} = \sqrt{\frac{C_0}{K_r + 1}} r_{m1k}^{-\frac{\beta_u}{2}} \tilde{h}_{m1k}, \quad (33)$$

$$[\mathbf{h}_k]_{(m-1)N+n} = h_{mnk}. \quad (34)$$

Furthermore,  $\mathbf{G} = \text{blkdiag}\{\mathbf{g}_1, \mathbf{g}_2, \dots, \mathbf{g}_M\} \in \mathbb{C}^{MN \times M}$  and  $\mathbf{\Xi} = \text{diag}\{\sqrt{\xi_{11}}, \dots, \sqrt{\xi_{1N}}, \sqrt{\xi_{21}}, \dots, \sqrt{\xi_{2N}}, \dots, \sqrt{\xi_{MN}}\} \in \mathbb{R}^{MN \times MN}$  denote the overall in-waveguide channel and PA power radiation matrices, respectively. The expectations in (31) can be calculated by

$$\mathbb{E} \left\{ |\bar{\mathbf{h}}_k^T \mathbf{\Xi} \mathbf{G} \mathbf{w}_k|^2 \right\} = \frac{C_0}{K_r + 1} \mathbf{w}_k^T \mathbf{G}^T \mathbf{\Xi}^T \mathbf{R}_k \mathbf{\Xi} \mathbf{G}^* \mathbf{w}_k^*, \quad (35)$$

$$\mathbb{E} \left\{ |\mathbf{h}_k^T \mathbf{\Xi} \mathbf{G} \mathbf{w}_i|^2 \right\} = \mathbf{w}_i^T \mathbf{G}^T \mathbf{\Xi}^T \bar{\mathbf{h}}_k \bar{\mathbf{h}}_k^H \mathbf{\Xi} \mathbf{G}^* \mathbf{w}_i^* + \frac{C_0}{K_r + 1} \mathbf{w}_i^T \mathbf{G}^T \mathbf{\Xi}^T \mathbf{R}_k \mathbf{\Xi} \mathbf{G}^* \mathbf{w}_i^*, \quad (36)$$

where  $\mathbf{R}_k = \text{diag}\{r_{11k}^{-\beta_u}, r_{12k}^{-\beta_u}, \dots, r_{1Nk}^{-\beta_u}, \dots, r_{m1k}^{-\beta_u}, r_{m2k}^{-\beta_u}, \dots, r_{mNk}^{-\beta_u}, \dots, r_{M1k}^{-\beta_u}, r_{M2k}^{-\beta_u}, \dots, r_{MNk}^{-\beta_u}\} \in \mathbb{R}^{MN \times MN}$ . Then, the achievable rate of the  $k$ -th user is given by (37).

The power consumption of PASS is primarily from  $M$  RF-chains and  $MN$  activated PAs, which is expressed as

$$P_{\text{all}} = \sum_{k=1}^K \frac{\|\mathbf{w}_k\|^2}{\nu} + P_{\text{BS}}^{\text{sta}} + MN \cdot P_{\text{PA}}, \quad (38)$$

where  $\nu > 0$  is the efficiency of the transmit power amplifier of RF-chains,  $P_{\text{BS}}^{\text{sta}}$  is the static power consumption of the RF-chains, mainly from circuit operation, cooling, and other static hardware overhead, and  $P_{\text{PA}}$  denotes the power consumption of each PA, given by

$$P_{\text{PA}} = \begin{cases} P_{\text{PA}}^{\text{act}} + P_{\text{PA}}^{\text{mot}} + P_{\text{PA}}^{\text{pie}}, & \text{for STT,} \\ P_{\text{PA}}^{\text{act}} + P_{\text{PA}}^{\text{mot}}, & \text{for STA,} \\ P_{\text{PA}}^{\text{act}} + P_{\text{PA}}^{\text{pie}}, & \text{for SAT,} \\ P_{\text{PA}}^{\text{act}}, & \text{for SAA.} \end{cases} \quad (39)$$

where  $P_{\text{PA}}^{\text{act}}$ ,  $P_{\text{PA}}^{\text{mot}}$ ,  $P_{\text{PA}}^{\text{pie}}$  denote the power consumption of the activation, motorized-module, piezoelectric-module equipment of each PA, respectively. Based on the derived achievable rate and power consumption model, the energy efficiency of PASS is expressed as

$$\eta_{EE} = \frac{B \cdot \sum_{k=1}^K R_k}{P_{\text{all}}}, \quad (40)$$

where  $B$  is transmission bandwidth, and  $R_k$  and  $P_{\text{all}}$  are given by Eqs. (37) and (38), respectively.

### C. Problem Formulation

Without loss of generality, it can be assumed that the  $M$  waveguides are deployed along the  $x$ -axis. Under this circumstance, the coordinate of the  $n$ -th PA on the  $m$ -th waveguide is given by  $\mathbf{p}_{mn} = [x_{mn}, \bar{Y}_m]$ , where  $\bar{Y}_m$  are known a priori,  $\forall m$ . The distance in channels (25) and (26) can be expressed as  $d_{mn} = x_{mn}$  and  $r_{mnk} = \sqrt{(x_k^U - x_{mn}^P)^2 + (y_k^U - \bar{Y}_m^P)^2}$ . The  $x$ -axis coordinates  $\mathbf{X}$  simultaneously affects  $\mathbf{G}$  and  $\mathbf{h}_k$  for  $\forall k$ , thereby influencing the energy efficiency of PASS, where  $\mathbf{X} = [\mathbf{x}_1, \mathbf{x}_2, \dots, \mathbf{x}_M] \in \mathbb{R}^{N \times M}$  and  $\mathbf{x}_m = [x_{m1}, x_{m2}, \dots, x_{mN}]^T$ . Under this setup, the EE maximization problem in the DSD framework for PASS can be formulated as

$$\max_{\mathbf{W}, \mathbf{\Xi}, \mathbf{X}} \eta_{EE} \quad (41a)$$

$$\text{s.t.} \quad \sum_{k=1}^K \|\mathbf{w}_k\|^2 \leq P_{\text{max}}, \quad (41b)$$

$$\xi_{mn} \geq 0, \quad \sum_{n=1}^N \xi_{mn} = 1, \quad \forall m, n, \quad (41c)$$

$$x_{mn} \in [x_m^{\min}, x_m^{\max}], \quad |x_{mn} - x_{mn'}| \geq \Delta x, \quad \forall m, n, n', \quad (41d)$$

where  $\mathbf{W} = [\mathbf{w}_1, \mathbf{w}_2, \dots, \mathbf{w}_K] \in \mathbb{C}^{M \times K}$  is the overall transmit precoding matrix,  $x_m^{\min}$  and  $x_m^{\max}$  denote the minimum and maximum coordinates of the sliding range of the  $m$ -th waveguide along the  $x$ -axis, respectively, and  $\Delta x$  is the minimum feasible spacing between any two PAs. The formulated problem presents significant challenges, primarily due to the intricate coupling of optimization variables and the inherent non-convexity of the objective function. First, the

$$R_k = \log_2 \left( 1 + \frac{|\bar{\mathbf{h}}_k^T \Xi \mathbf{G} \mathbf{w}_k|^2}{\frac{C_0}{K_r+1} \mathbf{w}_k^T \mathbf{G}^T \Xi^T \mathbf{R}_k \Xi \mathbf{G}^* \mathbf{w}_k^* + \sum_{i \neq k}^K \left( |\bar{\mathbf{h}}_k^T \Xi \mathbf{G} \mathbf{w}_i|^2 + \frac{C_0}{K_r+1} \mathbf{w}_i^T \mathbf{G}^T \Xi^T \mathbf{R}_k \Xi \mathbf{G}^* \mathbf{w}_i^* \right) + N_0} \right). \quad (37)$$

optimization variables  $\mathbf{W}$ ,  $\Xi$ , and  $\mathbf{X}$  are all mutually coupled in the objective function. Second, the objective function itself is highly non-convex, incorporating fractional and logarithmic terms that further complicate the PASS design. Moreover, the optimization over the  $MN$  PA positions  $\mathbf{X}$  non-linearly influences both the channel matrices  $\{\mathbf{h}_k\}_{k=1}^K$  and  $\mathbf{G}$ , introducing pervasive non-convexity in both the objective function and the constraints. To overcome these challenges, a penalty-based alternating optimization algorithm is proposed in the following under the DSD framework.

#### IV. ENERGY EFFICIENCY OPTIMIZATION DESIGN

This section will first address the non-convexity objective function of problem (41) by transforming it into a tractable polynomial expression, and propose a penalty-based alternating optimization algorithm to jointly optimize  $\mathbf{W}$ ,  $\Xi$ , and  $\mathbf{X}$  under the DSD framework.

##### A. Problem Reformulation

The objective function of problem (41) can be equivalently transformed into a convex function w.r.t.  $\mathbf{W}$ ,  $\Xi$ , and  $\mathbf{X}$  in the following lemma.

**Lemma 1.** The energy efficiency maximum problem can be transformed into

$$\begin{aligned} \min_{\mathbf{W}, \Xi, \mathbf{X}} \quad & B \cdot \sum_{k=1}^K \kappa_k \epsilon_k + q \cdot P_{all} \\ \text{s.t.} \quad & (41b), (41c), (41d), \end{aligned} \quad (42)$$

where the optimization variables are

$$\begin{aligned} \epsilon_k = & |t_k|^2 \sum_{i=1}^K \left( |\bar{\mathbf{h}}_k^T \Xi \mathbf{G} \mathbf{w}_i|^2 + \frac{C_0}{K_r+1} \mathbf{w}_i^T \mathbf{G}^T \Xi^T \mathbf{R}_k \Xi \mathbf{G}^* \mathbf{w}_i^* \right) \\ & - 2\Re \{ t_k^* \bar{\mathbf{h}}_k^T \Xi \mathbf{G} \mathbf{w}_k \} + |t_k|^2 N_0 + 1. \end{aligned} \quad (43)$$

Besides, the auxiliary variables  $\mathbf{t}$ ,  $\kappa$  and  $q$  are updated by

$$t_k = \frac{\bar{\mathbf{h}}_k^T \Xi \mathbf{G} \mathbf{w}_k}{\sum_{i=1}^K \left( |\bar{\mathbf{h}}_k^T \Xi \mathbf{G} \mathbf{w}_i|^2 + \frac{C_0}{K_r+1} \mathbf{w}_i^T \mathbf{G}^T \Xi^T \mathbf{R}_k \Xi \mathbf{G}^* \mathbf{w}_i^* \right) + N_0}, \quad (44)$$

$\kappa_k = \epsilon_k^{-1}$ , and  $q = \frac{B \cdot \sum_{k=1}^K R_k}{P_{all}}$  at every iteration.

*Proof:* Please see Appendix A.  $\square$

Subsequently, we aim to maximize the energy efficiency by jointly optimizing  $\mathbf{W}$ ,  $\Xi$ , and  $\mathbf{X}$ . However, it is still difficult to solve this problem due to the coupling effects among the optimization variables. Generally, there are no standard methods to obtain a joint optimal solution for these non-convex problems. One common method is to apply the alternating optimization by iteratively optimizing  $\mathbf{W}$ ,  $\Xi$ , and  $\mathbf{X}$  to solve the problem (42) with the other being fixed. As such, in the  $j$ -th iteration, we propose a Lagrange dual method to update  $\mathbf{W}^{(j)}$ , a multi-block manifold optimization to update  $\Xi^{(j)}$  and

penalty-based method to update  $\mathbf{X}^{(j)}$ . The detailed update procedures are provided in the following subsections.

##### B. Penalty-based Alternating Optimization Algorithm

1) *Subproblem w.r.t.  $\mathbf{W}$ :* With fixed  $\Xi$  and  $\mathbf{X}$ , by discarding the constant in objective function (42) irrelevant to  $\mathbf{W}$ , the optimization problem becomes

$$\min_{\mathbf{W}} f_1(\mathbf{W}) \quad (45a)$$

$$\text{s.t.} \quad (41b), \quad (45b)$$

where the objective function is given by

$$\begin{aligned} f_1(\mathbf{W}) = & B \cdot \sum_{i=1}^K \mathbf{w}_i^T \sum_{k=1}^K \kappa_k |t_k|^2 \left( \mathbf{G}^T \Xi^T \bar{\mathbf{h}}_k \bar{\mathbf{h}}_k^H \Xi \mathbf{G}^* \right. \\ & \left. + \frac{C_0}{K_r+1} \mathbf{G}^T \Xi^T \mathbf{R}_k \Xi \mathbf{G}^* \right) \mathbf{w}_i^* + \frac{q}{\nu} \sum_{k=1}^K \|\mathbf{w}_k\|^2 \\ & - \sum_{k=1}^K 2B\kappa_k \Re \{ t_k^* \bar{\mathbf{h}}_k^T \Xi \mathbf{G} \mathbf{w}_k \}. \end{aligned} \quad (46)$$

In addition, the constraint (41b) can be equivalently transformed as in the objective function, i.e.,

$$\min_{\mathbf{W}} f_1(\mathbf{W}) + \rho \left( \sum_{k=1}^K \|\mathbf{w}_k\|^2 - P_{\max} \right), \quad (47)$$

where  $\rho > 0$  is the Lagrange multiplier. Then, the objective function of problem (47) can be rewritten as

$$\min_{\mathbf{w}} \mathbf{w}^T \mathbf{A}_w \mathbf{w}^* - 2\Re \{ \zeta_w^T \mathbf{w} \}, \quad (48)$$

where  $\mathbf{w} = [\mathbf{w}_1^T, \mathbf{w}_2^T, \dots, \mathbf{w}_K^T]^T$ ,  $\mathbf{A}_w = \text{blkdiag}\{\mathbf{A}_{w1}, \mathbf{A}_{w2}, \dots, \mathbf{A}_{wK}\}$ , and  $\zeta_w = [\zeta_{w1}^T, \zeta_{w2}^T, \dots, \zeta_{wK}^T]^T$ . More specifically,  $\mathbf{A}_{wi}$  and  $\zeta_{w1}^T$  are defined by

$$\begin{aligned} \mathbf{A}_{wi} = & B \sum_{k=1}^K \kappa_k |t_k|^2 \left( \mathbf{G}^T \Xi^T \bar{\mathbf{h}}_k \bar{\mathbf{h}}_k^H \Xi \mathbf{G}^* \right. \\ & \left. + \frac{C_0}{K_r+1} \mathbf{G}^T \Xi^T \mathbf{R}_k \Xi \mathbf{G}^* \right) + \left( \frac{q}{\nu} + \rho \right) \mathbf{I}_M, \end{aligned} \quad (49)$$

$$\zeta_{wk}^T = B\kappa_k t_k^* \bar{\mathbf{h}}_k^T \Xi \mathbf{G}. \quad (50)$$

Since  $\mathbf{A}_w$  is a positive-definite matrix, the optimal  $\mathbf{w}$  can be obtained by setting the first-order derivative of the objective function (48) to zero, which yields

$$\mathbf{w} = (\mathbf{A}_w^T)^{-1} \zeta_w^*, \quad (51)$$

where the optimal  $\rho$  in  $\mathbf{A}_w$  is chosen by the Karush-Kuhn-Tucker condition of the Lagrange duality transformation. It can be determined efficiently through bisection search to satisfy

$$\rho = \min\{\rho > 0 : \sum_{k=1}^K \|\mathbf{w}_k\|^2 \leq P_{\max}\}. \quad (52)$$

2) *Subproblem w.r.t.  $\Xi$ :* With fixed  $\mathbf{W}$  and  $\mathbf{X}$ , by discarding the constant in objective function (42) irrelevant to  $\Xi$ , the

**Algorithm 1** Block Coordinate Manifold Optimization Algorithm for Updating  $\Xi^{(j)}$ .

- 
- 1: **Input:**  $\xi^{(0)} = \text{diag}^{-1}(\Xi^{(j)})$ .
  - 2: Set the inner iteration index  $r = 0$ .
  - 3: **repeat**
  - 4: Update  $\nabla_{\mathcal{M}} f_2(\xi_m^{(r)})$  by (55) and (56).
  - 5: Update  $\varpi_m^{(r+1)}$ ,  $\forall m$ , by the Armijo backtracking line search algorithm.
  - 6: Update  $\xi_m^{(r+1)}$  with  $\frac{\xi_m^{(r)} - \varpi_m^{(r+1)} \nabla_{\mathcal{M}} f_2(\xi_m^{(r)})}{\|\xi_m^{(r)} - \varpi_m^{(r+1)} \nabla_{\mathcal{M}} f_2(\xi_m^{(r)})\|}$
  - 7: Update  $r \leftarrow r + 1$ .
  - 8: **until** the fractional decrease of  $\|\xi\|^2$  falls below  $\epsilon_\xi$ .
  - 9: **Output:**  $\Xi^{(j+1)} = \text{diag}(\xi^{(r)})$ .
- 

optimization problem becomes

$$\begin{aligned} \min_{\xi} f_2(\xi) &= \xi^T \mathbf{A}_\xi \xi - 2 \sum_{k=1}^K \kappa_k \Re \left\{ t_k^* \bar{\mathbf{h}}_k^T \text{diag}(\mathbf{G} \mathbf{w}_k) \xi \right\} \\ \text{s.t.} \quad & (41\text{c}), \end{aligned} \quad (53)$$

where  $\xi \in \mathbb{R}^{MN \times 1}$  is composed of diagonal elements of  $\Xi$ , i.e.,  $\Xi = \text{diag}(\xi)$ , and

$$\begin{aligned} \mathbf{A}_\xi &= \sum_{i=1}^K \sum_{k=1}^K \kappa_k |t_k|^2 \left( \text{diag}(\mathbf{G} \mathbf{w}_i) \bar{\mathbf{h}}_k \bar{\mathbf{h}}_k^H \text{diag}(\mathbf{G}^* \mathbf{w}_i^*) \right. \\ &\quad \left. + \frac{C_0}{K_r + 1} \text{diag}(\mathbf{G} \mathbf{w}_i) \mathbf{R}_k \text{diag}(\mathbf{G}^* \mathbf{w}_i^*) \right). \end{aligned} \quad (54)$$

However, since the constraint (41c) is non-convex, problem (53) cannot be solved by a hand-on convex algorithm. We first rewrite the constraint (41c) into  $\|\xi_m\|^2 = 1$  for  $\forall m$ , where  $\xi_m = [\sqrt{\xi_{m1}}, \sqrt{\xi_{m2}}, \dots, \sqrt{\xi_{mN}}]^T$ . As such, the vector  $\xi_m$  should lie on the surface of a unit sphere. Thus, this problem naturally fits into the framework of manifold optimization. Let  $\mathcal{M}$  denote the Riemannian manifold used to define the constraints for  $\xi$ , which is given by  $\mathcal{M} = \{\xi \in \mathbb{R}^{MN \times 1} : \|\xi_m\|^2 = 1, \forall m\}$ .

It is worth noting that each block  $\xi_m$  in vector  $\xi$  should reside in a manifold space for  $\forall m$ . Hence, the update of  $\xi$  requires computing the Riemannian gradient [24] for each block individually to enforce their norm constraints inherently. Specifically, the Riemannian gradient of  $f_2(\xi)$  at  $\xi_m$ , denoted by  $\nabla_{\mathcal{M}} f_2(\xi_m)$ , can be obtained by orthogonally projecting the Euclidean gradient  $\nabla f_2(\xi_m)$ , i.e.,

$$\nabla_{\mathcal{M}} f_2(\xi_m) = \nabla f_2(\xi_m) - \text{tr}(\xi_m^T \nabla f_2(\xi_m)) \xi_m, \quad (55)$$

where the Euclidean gradient can be computed by  $\nabla f_2(\xi_m) = [\nabla f_2(\xi)]_{(m-1)N+1:mN}$  with

$$\nabla f_2(\xi) = (\mathbf{A}_\xi + \mathbf{A}_\xi^T) \xi - 2 \sum_{k=1}^K \Re \left\{ t_k^* \text{diag}(\mathbf{G} \mathbf{w}_k) \bar{\mathbf{h}}_k \right\}. \quad (56)$$

Finally, an additional operation is needed to map the vector  $\xi_m$  to the manifold  $\mathcal{M}$  by a retraction mapping operator, i.e.,

$$\xi_m \leftarrow \frac{\xi_m - \varpi_m \nabla_{\mathcal{M}} f_2(\xi_m)}{\|\xi_m - \varpi_m \nabla_{\mathcal{M}} f_2(\xi_m)\|}, \quad (57)$$

where  $\varpi_m$  is the descent step size and its value can be updated by the Armijo backtracking line search [25]. Then, the optimization w.r.t.  $\Xi$  is summarized in **Algorithm 1**.

3) *Subproblem w.r.t. X*: With fixed  $\mathbf{W}$  and  $\Xi$ , by discarding the constant in objective function (42) irrelevant to  $\mathbf{X}$ , the optimization problem becomes

$$\min_{\mathbf{X}} f_3(\mathbf{X}) \quad (58\text{a})$$

$$\text{s.t.} \quad (41\text{d}), \quad (58\text{b})$$

where the objective function is given by

$$\begin{aligned} f_3(\mathbf{X}) &= \sum_{i=1}^K \sum_{k=1}^K \kappa_k |t_k|^2 \xi^T \left( \underbrace{\text{diag}(\mathbf{G} \mathbf{w}_i) \bar{\mathbf{h}}_k \bar{\mathbf{h}}_k^H \text{diag}(\mathbf{G}^* \mathbf{w}_i^*)}_{A_1} \right. \\ &\quad \left. + \frac{C_0}{K_r + 1} \underbrace{\text{diag}(\mathbf{G} \mathbf{w}_i) \mathbf{R}_k \text{diag}(\mathbf{G}^* \mathbf{w}_i^*)}_{A_2} \right) \xi \\ &\quad - 2 \sum_{k=1}^K \kappa_k \Re \left\{ \underbrace{t_k^* \bar{\mathbf{h}}_k^T \text{diag}(\mathbf{G} \mathbf{w}_k)}_{A_3} \xi \right\}. \end{aligned} \quad (59)$$

Based on the proposed DSD framework in Section II, we introduce two auxiliary variables to represent the amplitude and phase components of the objective function (59) as

$$u_{mnk} = \exp(-\alpha_g x_{mn}) r_{mnk}^{-\frac{\beta_u}{2}}, \quad (60)$$

$$z_{mnk} = \exp\left(-j \frac{2\pi}{\lambda_g} x_{mn} - j \frac{2\pi}{\lambda} r_{mnk}\right). \quad (61)$$

Then, the objective function (59) can be rewritten through

$$A_1 = \frac{C_0 K_r}{K_r + 1} \text{diag}(\bar{\mathbf{w}}_i) (\mathbf{u}_k \circ \mathbf{z}_k) (\mathbf{u}_k \circ \mathbf{z}_k)^H \text{diag}(\bar{\mathbf{w}}_i^*), \quad (62)$$

$$A_2 = \text{diag}(\bar{\mathbf{w}}_i) \text{diag}(\mathbf{u}_k \circ \mathbf{u}_k^*) \text{diag}(\bar{\mathbf{w}}_i^*), \quad (63)$$

$$A_3 = t_k^* (\mathbf{u}_k \circ \mathbf{z}_k)^T \text{diag}(\bar{\mathbf{w}}_i), \quad (64)$$

where  $\bar{\mathbf{w}}_i = [w_{1i} \mathbf{1}_N^T, w_{2i} \mathbf{1}_N^T, \dots, w_{Mi} \mathbf{1}_N^T]^T$ ,  $\mathbf{u}_k = [u_{11k}, \dots, u_{1Nk}, \dots, u_{m1k}, u_{m2k}, \dots, u_{mNk}, \dots, u_{MNk}]^T$  and  $\mathbf{z}_k = [z_{11k}, \dots, z_{1Nk}, \dots, z_{m1k}, z_{m2k}, \dots, z_{mNk}, \dots, z_{MNk}]^T$ .

Thus, the optimization problem w.r.t.  $\mathbf{X}$  can be transformed into the problem of optimizing two independent vectors,  $\mathbf{u}$  and  $\mathbf{z}$ , through the proposed DSD design, as

$$\min_{\mathbf{u}, \mathbf{z}} f_4(\mathbf{u}, \mathbf{z}) \quad (65\text{a})$$

$$\text{s.t.} \quad \|z_{mnk}\| = 1, \text{ for } \forall m, n, k, \quad (65\text{b})$$

$$u_{mnk} = \exp(-\alpha_g x_{mn}) r_{mnk}^{-\frac{\beta_u}{2}}, \text{ for } \forall m, n, k, \quad (65\text{c})$$

$$(41\text{d}), \quad (65\text{d})$$

where  $\mathbf{u} = [\mathbf{u}_1^T, \mathbf{u}_2^T, \dots, \mathbf{u}_K^T]^T$ ,  $\mathbf{z} = [\mathbf{z}_1^T, \mathbf{z}_2^T, \dots, \mathbf{z}_K^T]^T$  and

$$\begin{aligned} f_4(\mathbf{u}, \mathbf{z}) &= \sum_{i=1}^K \sum_{k=1}^K \kappa_k |t_k|^2 \xi^T \left( \frac{C_0 K_r}{K_r + 1} \text{diag}(\bar{\mathbf{w}}_i) \right. \\ &\quad \times (\mathbf{u}_k \circ \mathbf{z}_k) (\mathbf{u}_k \circ \mathbf{z}_k)^H \text{diag}(\bar{\mathbf{w}}_i^*) \\ &\quad \left. + \frac{C_0}{K_r + 1} \text{diag}(\bar{\mathbf{w}}_i) \text{diag}(\mathbf{u}_k \circ \mathbf{u}_k^*) \text{diag}(\bar{\mathbf{w}}_i^*) \right) \xi \\ &\quad - 2 \sum_{k=1}^K \kappa_k \Re \left\{ t_k^* (\mathbf{u}_k \circ \mathbf{z}_k)^T \text{diag}(\bar{\mathbf{w}}_i) \xi \right\}. \end{aligned} \quad (66)$$

The constraints (65b) and (65c) are both non-convex to  $\mathbf{u}$  and  $\mathbf{z}$ , which hinder the effective solve of the problem (65). Hence, we introduce two auxiliary vector  $\mathbf{b}$  and  $\mathbf{c}$  with the equality of  $\mathbf{z} = \mathbf{c}$  and  $\mathbf{u} = \mathbf{b}$ . As such, the optimization problem (65) can be rewritten by replacing  $\mathbf{u}$  and  $\mathbf{z}$  with  $\mathbf{b}$

and  $\mathbf{c}$ , respectively, yielding

$$\min_{\mathbf{b}, \mathbf{c}, \mathbf{u}, \mathbf{z}} f_4(\mathbf{b}, \mathbf{c}) \quad (67a)$$

$$\text{s.t. } \mathbf{u} = \mathbf{b}, \quad (67b)$$

$$\mathbf{z} = \mathbf{c}, \quad (67c)$$

$$(41d), (65c), (65b). \quad (67d)$$

The augmented Lagrangian function of problem (67) can incorporate equality constraints into the objective function by introducing corresponding penalty terms [26], written as

$$\mathcal{L}(\mathbf{b}, \mathbf{u}, \mathbf{c}, \mathbf{z}) = f_4(\mathbf{b}, \mathbf{c}) + \varrho (\|\mathbf{u} - \mathbf{b}\|^2 + \|\mathbf{z} - \mathbf{c}\|^2), \quad (68)$$

where  $\varrho > 0$  is the quadratic penalty parameter of the equality constraints and updated in the outer iteration. Let  $(\mathbf{u}^{(0)}, \mathbf{b}^{(0)}, \mathbf{z}^{(0)}, \mathbf{c}^{(0)})$  be initial variables as feasible values. The proposed penalty-based method iteratively performs the following steps as

$$\begin{cases} \mathbf{b}^{(j+1)} = \arg \min_{\mathbf{b}} \mathcal{L}(\mathbf{b}, \mathbf{u}^{(j)}, \mathbf{c}^{(j)}, \mathbf{z}^{(j)}), \\ \mathbf{u}^{(j+1)} = \arg \min_{\mathbf{u}} \mathcal{L}(\mathbf{b}^{(j+1)}, \mathbf{u}, \mathbf{c}^{(j)}, \mathbf{z}^{(j)}), \\ \mathbf{c}^{(j+1)} = \arg \min_{\mathbf{c}} \mathcal{L}(\mathbf{b}^{(j+1)}, \mathbf{u}^{(j+1)}, \mathbf{c}, \mathbf{z}^{(j)}), \\ \mathbf{z}^{(j+1)} = \arg \min_{\mathbf{z}} \mathcal{L}(\mathbf{b}^{(j+1)}, \mathbf{u}^{(j+1)}, \mathbf{c}^{(j+1)}, \mathbf{z}). \end{cases} \quad (69)$$

Then, we will divide in into two subproblems for obtaining  $\{\mathbf{b}^{(j+1)}, \mathbf{u}^{(j+1)}\}$  and  $\{\mathbf{c}^{(j+1)}, \mathbf{z}^{(j+1)}\}$ .

• *Optimization of  $\{\mathbf{b}^{(j+1)}, \mathbf{u}^{(j+1)}\}$* : By dropping irrelevant variables, the optimization problem of this block becomes

$$\begin{aligned} \min_{\mathbf{b}, \mathbf{u}} \mathbf{b}^T \mathbf{A}_b \mathbf{b} - 2\Re \{ \boldsymbol{\zeta}_b^T \mathbf{b} \} + \varrho \|\mathbf{u} - \mathbf{b}\|^2 \\ \text{s.t. } (41d), (65c), \end{aligned} \quad (70)$$

where  $\mathbf{A}_b = \text{blkdiag}\{\mathbf{A}_{b1}, \mathbf{A}_{b2}, \dots, \mathbf{A}_{bK}\}$ ,  $\boldsymbol{\zeta}_b = [\boldsymbol{\zeta}_{b1}^T, \boldsymbol{\zeta}_{b2}^T, \dots, \boldsymbol{\zeta}_{bK}^T]^T$ ,  $\boldsymbol{\zeta}_{bk} = \kappa_k t_k^* \text{diag}(\mathbf{c}_k) \text{diag}(\bar{\mathbf{w}}_k) \boldsymbol{\xi}$ , and

$$\begin{aligned} \mathbf{A}_{bk} = \sum_{i=1}^K \kappa_k |t_k|^2 \text{diag}(\boldsymbol{\xi}) \text{diag}(\bar{\mathbf{w}}_i) \left( \frac{C_0 K_r}{K_r + 1} \mathbf{c}_k \mathbf{c}_k^H \right. \\ \left. + \frac{C_0}{K_r + 1} \mathbf{I}_{MN} \right) \text{diag}(\bar{\mathbf{w}}_i^*) \text{diag}(\boldsymbol{\xi}). \end{aligned} \quad (71)$$

It can be observed that the optimization problem (70) w.r.t.  $\mathbf{b}$  is an unconstrained least-squares problem, which can be solved optimally by setting its first-order derivative to zero and yielding

$$\mathbf{b} = (\mathbf{A}_b + \mathbf{A}_b^T + 2\varrho \mathbf{I}_{MNK})^{-1} (2\boldsymbol{\zeta}_b^* + 2\varrho \mathbf{u}). \quad (72)$$

The update of  $\mathbf{u}$  should satisfy the constraint (65c) and minimize the equality penalty term of the objective function (70). This can be efficiently solved through a one-dimensional search over the coarse grid set  $\mathbf{x}_m^{CG}$ . In particular, the design of  $\mathbf{x}_m^{CG}$  ensures that the grid values lie within  $[x_m^{\min}, x_m^{\max}]$  and that any two grid points are separated by at least  $\Delta x$ , thereby naturally satisfying constraint (41d). For  $\forall m, n$ , a one-

dimensional search for coarse grids is performed by

$$\begin{aligned} x_{mn}^C = \arg \min_{x_{mn} \in \mathbf{x}_m^{CG}} \sum_{k=1}^K \left| [\mathbf{b}]_{mnk} - \exp(-\alpha_g x_{mn}) \right. \\ \left. \times [(x_k^U - x_{mn})^2 + (y_k^U - \bar{Y}_m)^2]^{-\frac{\beta_g}{4}} \right|^2, \end{aligned} \quad (73)$$

where  $x_{mn}^C \neq x_{mn'}^C$ , for  $\forall n, n'$ . Then, the update of  $\mathbf{u}$  is given for  $\forall m, n, k$  by

$$\begin{aligned} [\mathbf{u}]_{mnk} = \exp(-\alpha_g x_{mn}^C) \\ \times [(x_k^U - x_{mn}^C)^2 + (y_k^U - \bar{Y}_m)^2]^{-\frac{\beta_g}{4}}. \end{aligned} \quad (74)$$

• *Optimization of  $\{\mathbf{c}^{(j+1)}, \mathbf{z}^{(j+1)}\}$* : By dropping irrelevant variables, the optimization problem of this block becomes

$$\min_{\mathbf{c}, \mathbf{z}} \mathbf{c}^T \mathbf{A}_c \mathbf{c}^* - 2\Re \{ \boldsymbol{\zeta}_c^T \mathbf{c} \} + \varrho \|\mathbf{z} - \mathbf{c}\|^2 \quad (75a)$$

$$\text{s.t. } (65b), \quad (75b)$$

where  $\mathbf{A}_c = \text{blkdiag}\{\mathbf{A}_{c1}, \mathbf{A}_{c2}, \dots, \mathbf{A}_{cK}\}$ ,  $\boldsymbol{\zeta}_c = [\boldsymbol{\zeta}_{c1}^T, \boldsymbol{\zeta}_{c2}^T, \dots, \boldsymbol{\zeta}_{cK}^T]^T$ ,  $\boldsymbol{\zeta}_{ck} = \kappa_k t_k^* \text{diag}(\mathbf{b}_k) \text{diag}(\bar{\mathbf{w}}_k) \boldsymbol{\xi}$ , and

$$\begin{aligned} \mathbf{A}_{ck} = \frac{C_0 K_r}{K_r + 1} \sum_{i=1}^K \kappa_k |t_k|^2 \text{diag}(\boldsymbol{\xi}) \text{diag}(\bar{\mathbf{w}}_i) \mathbf{b}_k \\ \times \mathbf{b}_k^H \text{diag}(\bar{\mathbf{w}}_i^*) \text{diag}(\boldsymbol{\xi}). \end{aligned} \quad (76)$$

Similarly, the optimization (75) w.r.t.  $\mathbf{c}$  is an unconstrained least-squares problem, which can be solved optimally by setting its first-order derivative to zero and yielding

$$\mathbf{c}^{(j+1)} = (\mathbf{A}_c^T + \varrho \mathbf{I}_{MNK})^{-1} (\boldsymbol{\zeta}_c^* + \varrho \mathbf{z}^{(j)}). \quad (77)$$

The update of  $\mathbf{z}$  should satisfy the constraint (65b) and minimize the equality penalty term of the objective function (75). This can also be efficiently solved through a one-dimensional search over the fine grid set  $\mathbf{x}_m^{FG}$ . For  $\forall m, n$ , a one-dimensional search for fine grids is performed by

$$\begin{aligned} \Delta x_{mn}^F = \arg \min_{\Delta x_{mn} \in \mathbf{x}_m^{FG}} \sum_{k=1}^K \left| [\mathbf{c}]_{mnk} - \exp\left(-j \frac{2\pi}{\lambda_g} (x_{mn}^C + \Delta x_{mn})\right) \right. \\ \left. - j \frac{2\pi}{\lambda} \sqrt{(x_k^U - (x_{mn}^C + \Delta x_{mn}))^2 + (y_k^U - \bar{Y}_m)^2} \right|^2. \end{aligned} \quad (78)$$

Then, the update of  $\mathbf{z}$  is given for  $\forall m, n, k$  by

$$\begin{aligned} [\mathbf{z}]_{mnk} = \exp\left(-j \frac{2\pi}{\lambda_g} (x_{mn}^C + \Delta x_{mn}^F)\right) \\ - j \frac{2\pi}{\lambda} \sqrt{(x_k^U - (x_{mn}^C + \Delta x_{mn}^F))^2 + (y_k^U - \bar{Y}_m)^2}. \end{aligned} \quad (79)$$

**Remark 2.** In the proposed DSD framework, the two-stage approach performs two sequential one-dimensional searches with total complexity on the order  $\mathcal{O}(G_C + G_F)$ , where  $G_C$  and  $G_F$  are the search grids number of coarse-stage and refinement-stage, respectively. It substantially reduces the computational complexity compared with prior methods whose joint search [14] has complexity on the order of  $\mathcal{O}(G_C G_F)$ .

The overall algorithm for joint transmit precoding, PA power radiation, and PA deployment is summarized in **Al-**

**Algorithm 2** Proposed Alternating Optimization Algorithm for Joint BS Transmit Precoding, PA Power Radiation, and PA Positioning.

- 1: Initialize equal power radiation and equal-interval position deployment for PAs, i.e.,  $\Xi^{(0)} = \sqrt{\frac{1}{N}} \mathbf{I}_{MN}$  and  $x_{mn}^{(0)} = \frac{x_m^{\max} - x_m^{\min}}{N+1} n$ . Initialize the precoding matrix  $\mathbf{W}^{(0)}$  by MRT scheme. Initialize  $\rho^{(0)} = 0$ .
- 2: **repeat**
- 3:   Set the iteration index  $j = 0$ .
- 4:   **repeat**
- 5:     Update  $t_k^{(j+1)}$ ,  $\kappa_k^{(j+1)}$ , for  $\forall k$ , and  $q^{(j+1)}$  by **Lemma 1**.
- 6:     Update  $\mathbf{W}^{(j+1)}$  as (51).
- 7:     Update  $\rho^{(j+1)}$  as (52).
- 8:     Update  $\Xi^{(j+1)}$  by **Algorithm 1**.
- 9:     Update  $\mathbf{b}^{(j+1)}$  and  $\mathbf{u}^{(j+1)}$  as (72) and (74), respectively.
- 10:    Update  $\mathbf{c}^{(j+1)}$  and  $\mathbf{z}^{(j+1)}$  as Eqs. (77) and (79), respectively.
- 11:    Update  $x_{mn}^{(j+1)} = x_{mn}^C + \Delta x_{mn}^F$  by Eqs. (73) and (78), for  $\forall m, n$ .
- 12:    Update  $j \leftarrow j + 1$ .
- 13:    **until** the fractional decrease of the objective value of  $\eta_{EE}$  falls below a predefined threshold  $\epsilon_{\text{in}}$
- 14:    Update the penalty factor  $\varrho \leftarrow c_\varrho \cdot \varrho$ .
- 15:    **until** the fractional decrease of the objective value of  $\eta_{EE}$  falls below a predefined threshold  $\epsilon_{\text{out}}$
- 16:    **Output:** The BS transmit precoding  $\mathbf{W}^{(j+1)}$ , PA radiation power allocation  $\Xi^{(j+1)}$ , PA position  $\mathbf{X}^{(j+1)}$ .

**Algorithm 2.** The four implementation protocols detailed in Section II can all be readily accommodated in **Algorithm 2**. More particularly, the analytical expressions of  $\mathbf{x}_m^{CG}$  and  $\mathbf{x}_m^{FG}$  for protocols (a)-(d) can be obtained from Eqs. (15) to (21) with well-designed  $\delta^F$  and  $\delta^C$ .

## V. NUMERICAL RESULTS

In this section, we will demonstrate the advantages of PASS and the effectiveness of the proposed algorithms in the proposed DSD framework. In particular, we consider the scenario over a square dense urban area of size  $100 \times 100 \text{ m}^2$ . The waveguides are uniformly arranged to serve randomly distributed users. Then, the position of deployed PA on the  $m$ -th waveguide can be expressed as  $\bar{Y}_m = \frac{100}{M+1} m$ ,  $x_m^{\min} = 0$  and  $x_m^{\max} = 100$ , for  $\forall m$ . Unless stated otherwise, the simulation setup is given in Table II.

### A. Validation of Derived Theoretical Results

Fig. 3 validates the theoretical results of energy efficiency given in (40), where the transmit precoding  $\mathbf{W}$  is obtained by the maximum ratio transmission scheme [27], and both the PAs' radiation power allocation and their positions are uniformly generated. Across all  $P_{\max}$ ,  $M$ , and  $N$ , the theoretical results, indicated by circular markers, closely overlap with the Monte Carlo curves, thereby confirming the accuracy of the derived energy efficiency expression. It can also be

Parameters	Values
Number of waveguides	$M = 3$
PA number per waveguide	$N = 4$
Transmission bandwidth	$B = 180 \text{ MHz}$
Number of users	$K = 4$
Position of users	$\mathbf{p}_1^U = [15.9, 54.3]$ , $\mathbf{p}_2^U = [98.6, 85.4]$ , $\mathbf{p}_3^U = [74.5, 24.1]$ , $\mathbf{p}_4^U = [37.4, 23.9]$
Carrier frequency and wavelength	$f_c = 28 \text{ GHz}$ , $\lambda = \frac{c}{f_c} = 1.07 \times 10^{-2}$ $\text{m}$ , $\lambda_g = \frac{\lambda}{1.4} = 7.65 \times 10^{-2} \text{ m}$
Rician factor	$K_r = 0.5$
In-waveguide attenuation	$\alpha_g = -18 \text{ dB}$
Wireless attenuation	$C_0 = \left(\frac{\lambda}{4\pi}\right)^2 = -61.4 \text{ dB}$ , $\beta_u = 2.2$
Transmit power efficiency	$\nu = 0.9$
Each PA activation power consumption	$P_{\text{PA}}^{\text{act}} = 5 \text{ dBm}$
Each PA motorized module power consumption	$P_{\text{PA}}^{\text{mot}} = 20 \text{ dBm}$
Each PA piezoelectric module power consumption	$P_{\text{PA}}^{\text{pie}} = 8 \text{ dBm}$
Static BS power consumption	$P_{\text{BS}}^{\text{sta}} = 9 \text{ dB}$
Noise power	$N_0 = -80 \text{ dBm}$
Initial step size	$\varrho_m^{(0)} = 10^2$
Predefined thresholds	$\epsilon_\epsilon = 10^{-4}$ , $\epsilon_{\text{in}} = \epsilon_{\text{out}} = 10^{-8}$
PA's sliding length	$L^C = 0.2 \text{ m}$
Positioning accuracy of PBs and PAs	$\delta^C = 1 \text{ m}$ , $\delta^F = 10^{-4} \text{ m}$

TABLE II: Simulation parameters and values.

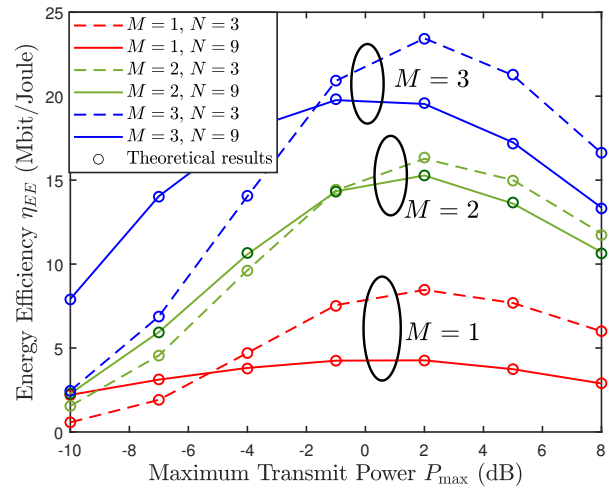


Fig. 3: Theoretical results of energy efficiency with Monte Carlo results.

observed that increasing  $M$  yields significant performance gains, whereas continuously increasing  $P_{\max}$  and  $N$  degrades energy efficiency. This arises from the fact that adding more waveguides enhances the spatial diversity gain, while increasing the transmit power or the PA number, in this non-optimized setting, brings only marginal spectral-efficiency improvements but substantially higher power consumption. These observations highlight the necessity of jointly designing transmit precoding, PA radiation power allocation, and PA deployment to fully realize the energy efficiency potential of PASS.

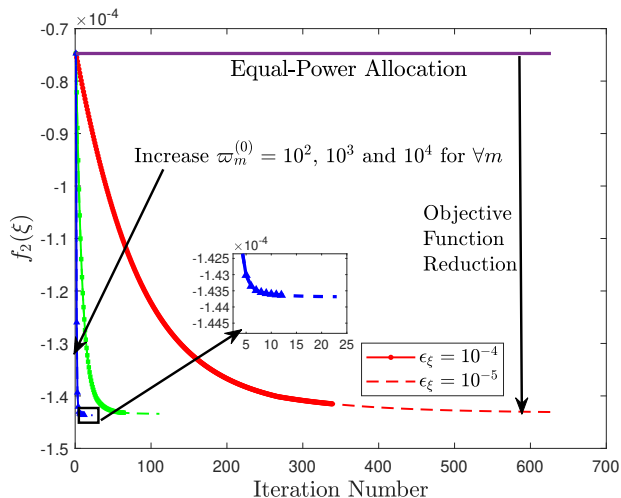
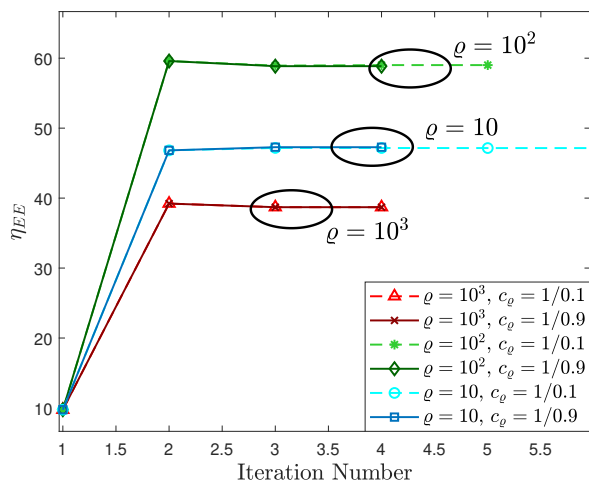
(a) Convergence behavior of  $\xi$ (b) Convergence behavior of  $\eta_{EE}$ 

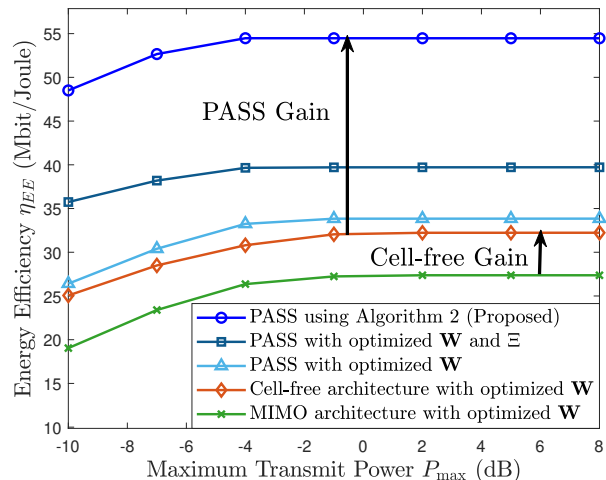
Fig. 4: Convergence behavior of Algorithm 1 and 2.

### B. Convergence Analysis of the Proposed Algorithm

Fig. 4 demonstrates the convergence behavior of the proposed algorithm. In particular, Fig. 4(a) verifies the convergence of **Algorithm 1** within the inner iteration loop. It shows that under different settings of  $\varpi^{(0)}$  and  $\epsilon_\xi$ , the objective function  $f_2(\xi)$  converges to the same value and all achieve substantial performance gains over equal-power allocation. Besides, with a proper choice of initial step size to  $10^2$ , the iteration number can be reduced by nearly 60-fold. Moreover, it is observed in Fig. 4(b) that after the first iteration of **Algorithm 2**, the energy efficiency already reaches the same level as the final performance, and converges within only a few subsequent iterations.

### C. Energy Efficiency Comparison: PASS vs. Conventional MIMO and Cell-Free Systems

Fig. 5 considers conventional MIMO and cell-free architectures as performance benchmarks. For a fair comparison, it is assumed that these two architectures employ the same number

Fig. 5: Comparison with MIMO and cell-free architectures, for  $\rho = 230$  and  $c_\rho = 1/0.9$ .

$M$  of RF chains and transmit precoding scheme as in PASS. Due to space limitations, we only present the received signal of the  $k$ -th user for the MIMO and cell-free as

$$y_k^{\text{MIMO}} = (\mathbf{h}_k^{\text{MIMO}})^T \sum_{i=1}^K \mathbf{w}_i^{\text{MIMO}} s_i + n_k, \quad (80)$$

$$y_k^{\text{cell-free}} = \sum_{m=1}^M (\mathbf{h}_{mk}^{\text{cell-free}})^T \sum_{i=1}^K \mathbf{w}_{mi}^{\text{cell-free}} s_i + n_k \quad (81)$$

where  $\mathbf{h}_k^{\text{MIMO}} \in \mathbb{C}^{M \times 1}$  and  $\mathbf{h}_{mk}^{\text{cell-free}} \in \mathbb{C}^{N \times 1}$  are the channel from the  $k$ -th user to the MIMO-BS and to the  $m$ -th cell-free-BS, respectively. The MIMO-BS is positioned at  $(0, 0)$ , while the  $m$ -th cell-free-BS is positioned at  $(50, \frac{100}{M+1}m)$ .

It can be observed in the Fig. 5 that, as  $P_{\max}$  increases, all the energy efficiency curves first rise and then approach saturation. Specifically at  $P_{\max} = 5$  dB, the cell-free architecture achieves 17.7% higher energy efficiency than conventional MIMO, by virtue of spatial diversity gain from the cooperation of  $M$  BSs. Because PASS adopts a more distributed architecture, the third curve in Fig. 5 already exhibits performance gains under the same configuration. By further optimizing the PA radiation power allocation and the positions, a larger energy efficiency gain is achieved, yielding an additional improvement of about 70% w.r.t. the cell-free architecture.

### D. Impact of Waveguide and PA Numbers

Fig. 6 presents the energy efficiency of the proposed algorithm applied to PASS across  $M$  and  $N$ , exhibiting a markedly different trend and performance gain from Fig. 3. For instance, under  $(M, N, P_{\max}) = (3, 9, -2$  dB), the proposed algorithm achieves a 242.7% increase in energy efficiency compared with the baseline. Moreover, the curves in Fig. 6 do not exhibit the decreasing trend with increasing  $N$  and  $P_{\max}$  observed in Fig. 3. This benefit arises from the carefully designed transmit precoding and PA radiation power allocation in **Algorithm 2**, which can enhance system performance under a limited power budget.

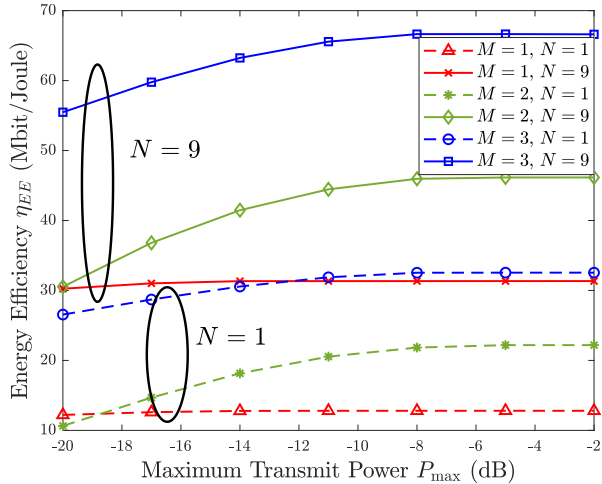


Fig. 6: Energy efficiency in Algorithm 2 under different number of waveguides and PAs, for  $\rho = 200$  and  $c_\rho = 1/0.5$ .

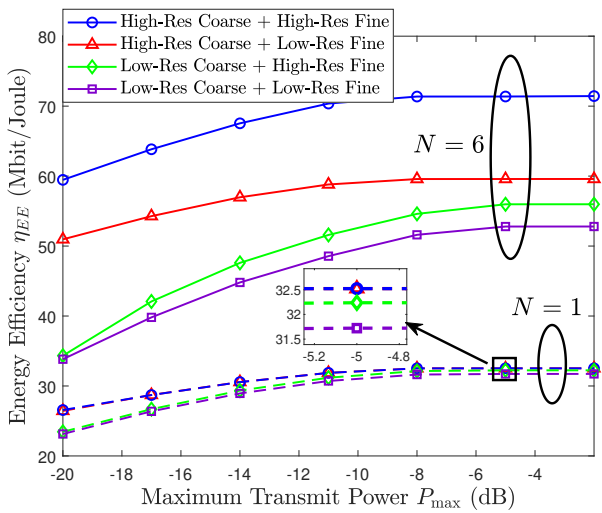


Fig. 7: Comparison under high and low resolution for coarse-sliding and fine-tuning grids, for  $\rho = 90$  and  $c_\rho = 1/0.6$ .

### E. Impact of Tuning Grid Resolution

Fig. 7 compares the energy efficiency of coarse-sliding under high-resolution  $\delta_C = 1$  m and low-resolution  $\delta_C = 10$  m, as well as fine-tuning under high-resolution  $\delta_F = 10^{-4}$  m and low-resolution  $\delta_F = 10^{-2}$  m. It can be observed in the single-PA scenario, the resolution of coarse-sliding and fine-tuning has a minor impact on communication performance. However, when  $N = 6$ , the resolution of PA position deployment has a pronounced effect on the overall energy efficiency. This is because the  $N$  PAs induce multi-path effects for each user, and inaccurate PA positions lead to phase misalignment among paths, resulting in substantial performance loss. Moreover, it shows that high-resolution in coarse-sliding is more critical than in fine-tuning, offering important guidance for selecting the motorized- and piezoelectric-based resolutions in the STT protocol.

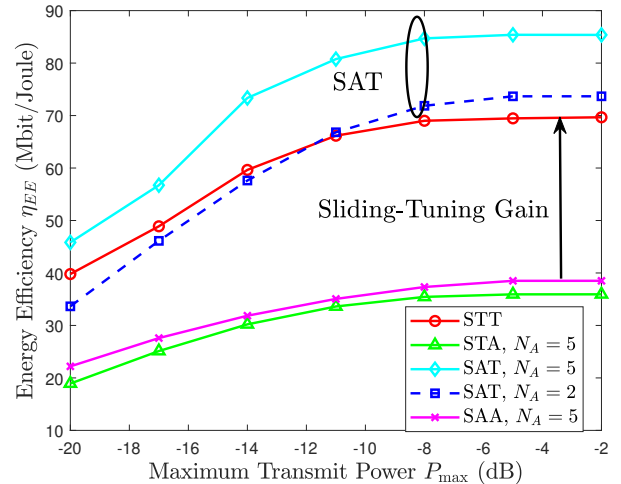


Fig. 8: Comparison under different protocols, for  $\rho = 450$  and  $c_\rho = 1/0.6$ .

### F. Energy Efficiency Performance of the Proposed Protocols

Fig. 8 demonstrates the energy efficiency of the proposed four protocols under varying  $P_{\max}$ . It is surprising that, although STT has the maximum DoF in PA position adjustment and is expected to deliver the best communication performance, it does not achieve the highest energy efficiency. Instead, SAT achieves the highest energy efficiency by eliminating the substantial motorized-module power consumption incurred during base sliding, which makes it an energy-efficient protocol worthy of further investigation within PASS. Notably, the SAT protocol can achieve comparable energy efficiency to STT by pre-deploying only twice as many bases, i.e.,  $N_C = 2$ . In contrast, the STA protocol incurs the base-sliding energy cost and simultaneously delivers unsatisfactory spectral efficiency, leading to the lowest energy efficiency. Compared with the SAA protocol, the STT protocol attains 80.8% improvement in energy efficiency, evidencing a clear performance gain from coarse-sliding and fine-tuning.

## VI. CONCLUSION

This paper has provided four implementation protocols in the DSD framework and proposed a novel low-complexity energy efficiency maximization algorithm, serving as a valuable reference for future PASS research and implementation. The proposed algorithm integrated Lagrangian transformations, block coordinate manifold optimization, and penalty-based alternating optimization to enable joint PASS design under each implementation protocol. Numerical results demonstrated substantial system gains with the proposed algorithm in PASS, and SAT was identified as the recommended protocol owing to its highest energy efficiency.

The proposed DSD framework for energy-efficient PA deployment could motivate future research on PASS, such as protocol design and channel estimation. More specifically, designing an appropriate protocol in the DSD framework for PASS is a promising direction for achieving an optimal trade-off among system performance, power consumption, and response time. It could also explicitly account for dual-scale

position adjustment speeds together with practical hardware constraints. In addition, dual-scale channel estimation and codebook design call for further investigation to accurately acquire CSI for this hybrid architecture.

#### APPENDIX A PROOF FOR LEMMA 1

The derivation process is based on the work [28], [29], which aims to transform the objective function equivalently by introducing some auxiliary variables. We first use the Dinkelbach's transform [30] to reformulate the objective function (41a) into

$$\max_{\mathbf{W}, \Xi, \mathbf{X}} B \cdot \sum_{k=1}^K R_k - q \cdot P_{all}, \quad (82)$$

with a new auxiliary variable  $q$  and iteratively updated by  $q = B \cdot \sum_{k=1}^K R_k / P_{all}$ . Then, we construct a new optimization problem and prove its equivalence to the problem (82) as

$$\min_{\mathbf{W}, \Xi, \mathbf{X}, \kappa, \mathbf{t}} B \cdot \sum_{k=1}^K (\kappa_k \epsilon_k - \log_2(\kappa_k)) + q \cdot P_{all} \quad (83a)$$

$$\text{s.t. (41b), (41c), (41d),} \quad (83b)$$

where  $\epsilon = [\epsilon_1, \dots, \epsilon_K]^T$  is given by (43). It can be observed that the variables  $\kappa_k$  and  $t_k$  for  $\forall k$  are concave to the objective function of (83), since their second-order derivatives are both greater than zero. Thus, the optimal  $\kappa$  and  $\mathbf{t}$  to solve the problem (83) can be obtained by setting their first-order derivatives to zero,  $\forall k$ , yielding  $\kappa_k = \epsilon_k^{-1}$  and

$$t_k = \frac{\bar{\mathbf{h}}_k^T \Xi \mathbf{G} \mathbf{w}_k}{\sum_{i=1}^K \left( \left| \bar{\mathbf{h}}_k^T \Xi \mathbf{G} \mathbf{w}_i \right|^2 + \frac{C_0}{K_\tau + 1} \mathbf{w}_i^T \mathbf{G}^T \Xi^T \mathbf{R}_k \Xi \mathbf{G}^* \mathbf{w}_i^* \right) + N_0}. \quad (84)$$

Then, we substitute the optimal  $\kappa$  and  $\mathbf{t}$  into the objective function of problem (83) and obtain

$$\min_{\mathbf{W}, \Xi, \mathbf{X}} B \cdot \sum_{k=1}^K (1 - \log_2(\epsilon_k^{-1})) + q \cdot P_{all}, \quad (85)$$

which can be proven to be equivalent to (82). Hence, for fixed optimal  $\kappa$  and  $\mathbf{t}$ , and dropping irrelevant constant terms w.r.t.  $\{\mathbf{W}, \Xi, \mathbf{X}\}$  in the objective function of (83), the problem (83) reduces to problem (42).

#### REFERENCES

- [1] ITU-R, *Framework and Overall Objectives of the Future Development of IMT for 2030 and Beyond*, Recommendation ITU-R M.2160-0, Nov. 2023. [Online]. Available: <https://www.itu.int/rec/R-REC-M.2160-0-202311-I/en>
- [2] C. Huang, A. Zappone, G. C. Alexandropoulos, M. Debbah and C. Yuen, "Reconfigurable intelligent surfaces for energy efficiency in wireless communication," *IEEE Trans. Wireless Commun.*, vol. 18, no. 8, pp. 4157-4170, Aug. 2019.
- [3] Q. Wu, and R. Zhang, "Intelligent reflecting surface enhanced wireless network via joint active and passive beamforming," *IEEE Trans. Wireless Commun.*, vol. 18, no. 11, pp. 5394-5409, Nov. 2019.
- [4] K. -K. Wong, A. Shojaefard, K. -F. Tong and Y. Zhang, "Fluid antenna systems," *IEEE Trans. Wireless Commun.*, vol. 20, no. 3, pp. 1950-1962, Mar. 2021.
- [5] T. Wu, K. Zhi, J. Yao, X. Lai, J. Zheng, H. Niu, M. Elkhashlan, K. -K Wong, C. -B. Chae, Z. Ding, G. K. Karagiannidis, M. Debbah, C. Yuen, "Fluid Antenna Systems Enabling 6G: Principles, Applications, and Research Directions", *arXiv preprint arXiv:2412.03839*, 2024.

- [6] L. Zhu et al., "A tutorial on movable antennas for wireless networks," *IEEE Commun. Surv. Tutor.*, early access, Feb. 2025, doi: 10.1109/COMST.2025.3546373.
- [7] Y. Liu, Z. Wang, X. Mu, C. Ouyang, X. Xu and Z. Ding, "Pinching-antenna systems: Architecture designs, opportunities, and outlook," *IEEE Commun. Mag.*, early access, 2025. doi: 10.1109/MCOM.001.2500037.
- [8] Z. Ding, R. Schober and H. Vincent Poor, "Flexible-antenna systems: A pinching-antenna perspective," *IEEE Trans. Wireless Commun.*, early access, 2025. doi: 10.1109/TCOMM.2025.3555866.
- [9] Y. Liu, H. Jiang, X. Xu, Z. Wang, J. Guo, C. Ouyang, X. Mu, Z. Ding, A. Nallanathan, G. K. Karagiannidis, R. Schober, "Pinching-antenna systems (PASS): A tutorial", *arXiv preprint arXiv:2508.07572*, 2025.
- [10] K. Wang, C. Ouyang, Y. Liu and Z. Ding, "Pinching-antenna systems with LoS blockages," *IEEE Wireless Commun. Lett.*, early access, 2025, doi: 10.1109/LWC.2025.3614451.
- [11] M. Sun, C. Ouyang, S. Wu, Y. Liu, "Physical layer security for pinching-antenna systems (PASS)," *IEEE Trans. Wireless Commun.*, early access, 2025.
- [12] K. Wang, Z. Ding, N. Al-Dahir, "Pinching-antenna systems for physical layer security," *IEEE Wireless Commun. Lett.*, early access, 2025, doi: 10.1109/LWC.2025.3624885.
- [13] A. Fukuda, H. Yamamoto, H. Okazaki, Y. Suzuki, and K. Kawai, "Pinching antenna - using a dielectric waveguide as an antenna," *NTT DOCOMO Technical J.*, vol. 23, no. 3, pp. 5-12, Jan. 2022.
- [14] Z. Wang, C. Ouyang, X. Mu, Y. Liu, Z. Ding, "Modeling and beamforming optimization for pinching-antenna systems", *IEEE Trans. Commun.*, early access, 2025, doi: 10.1109/TCOMM.2025.3621049.
- [15] S. Shan, C. Ouyang, Y. Li, Y. Liu, "Exploiting pinching-antenna systems in multicast communications," *IEEE Trans. Commun.*, early access, 2025.
- [16] J. -C. Chen, P. -C. Wu and K. -K. Wong, "Dynamic placement of pinching antennas for multicast MU-MISO downlinks," *IEEE Open J. Commun. Soc.*, vol. 6, pp. 5611-5625, Jun. 2025.
- [17] Y. Xu, D. Xu, X. Yu, S. Song, Z. Ding, R. Schober, "Joint radiation power, antenna position, and beamforming optimization for pinching-antenna systems with motion power consumption," *arXiv preprint arXiv:2507.02348*, 2025.
- [18] X. Xu, X. Mu, Z. Wang, Y. Liu, A. Nallanathan, "Pinching-antenna systems (PASS): Power radiation model and optimal beamforming design," *arXiv preprint arXiv:2505.00218*, 2025.
- [19] B. Zhang, H. Zhang, K. Yang, Y. Zhao, K. Wang, "On the performance analysis of pinching-antenna-enabled SWIPT systems," *arXiv preprint arXiv:2509.03836*, 2025.
- [20] D. K. Cheng, *Field and wave electromagnetics*, Addison-Wesley, 1989.
- [21] Physik Instrumente (PI) GmbH & Co. KG, *Miniature Precision Positioning Stages*. PI Catalog, 2015. Available: [https://www.pi-usa.us/fileadmin/user\\_upload/pi\\_us/files/catalogs/PI\\_Precision\\_Miniature\\_Translation\\_Stages.pdf](https://www.pi-usa.us/fileadmin/user_upload/pi_us/files/catalogs/PI_Precision_Miniature_Translation_Stages.pdf)
- [22] S. Parkvall, E. Dahlman, A. Furuskar and M. Frenne, "NR: The new 5G radio access technology," *IEEE Commun. Stand. Mag.*, vol. 1, no. 4, pp. 24-30, Dec. 2017.
- [23] H. Q. Ngo, A. Ashikhmin, H. Yang, E. G. Larsson and T. L. Marzetta, "Cell-free massive MIMO versus small cells," *IEEE Trans. Wireless Commun.*, vol. 16, no. 3, pp. 1834-1850, Mar. 2017.
- [24] P.-A. Absil, R. Mahony, and R. Sepulchre, *Optimization Algorithms on Matrix Manifolds*. Princeton, NJ, USA: Princeton Univ. Press, 2009.
- [25] S. Hosseini, W. Huang, and R. Yousefpour, "Line search algorithms for locally Lipschitz functions on Riemannian manifolds," *SIAM J. Optimization*, vol. 28, no. 1, pp. 596-619, 2018.
- [26] Q. Shi and M. Hong, "Penalty dual decomposition method for non-smooth nonconvex optimization—Part I: Algorithms and convergence analysis," *IEEE Trans. Signal Process.*, vol. 68, pp. 4108-4122, Jun. 2020.
- [27] X. Gan, C. Zhong, C. Huang, Z. Yang and Z. Zhang, "Multiple RISs assisted cell-free networks with two-timescale CSI: Performance analysis and system design," *IEEE Trans. Commun.*, vol. 70, no. 11, pp. 7696-7710, Nov. 2022.
- [28] K. Shen and W. Yu, "Fractional programming for communication systems—Part I: Power control and beamforming," *IEEE Trans. Signal Process.*, vol. 66, no. 10, pp. 2616-2630, May 2018.
- [29] Q. Shi, M. Razaviyayn, Z. -Q. Luo and C. He, "An iteratively weighted MMSE approach to distributed sum-utility maximization for a MIMO interfering broadcast channel," *IEEE Trans. Signal Process.*, vol. 59, no. 9, pp. 4331-4340, Sept. 2011.
- [30] W. Dinkelbach, "On nonlinear fractional programming," *Manage. Sci.*, vol. 133, no. 7, pp. 492-498, Mar. 1967.